# Probing the Acetylcholinesterase Inhibition of Sarin: A Comparative Interaction Study of the Inhibitor and Acetylcholine with a Model Enzyme Cavity

**D. Majumdar,[†] Szczepan Roszak,[‡] and Jerzy Leszczynski*[,†]**

*Computational Center for Molecular Structure and Interactions, Department of Chemistry, Jackson State University, Jackson, Mississippi 39217, and Institute of Physical and Theoretical Chemistry, Wroclaw University of Technology, Wybrzeże Wyspiańskiego 27, 50-370 Wroclaw, Poland*

*Received: March 10, 2006; In Final Form: May 12, 2006*

Interaction energies have been estimated between sarin and a model enzyme cavity of acetylcholinesterase (ACHE) using the density functional and Møller−Plesset second-order perturbation (MP2) levels of theories. The calculated interaction energies have been compared with those of acetylcholine and the same model ACHE cavity. The ACHE···sarin and ACHE···acetylcholine (Ach) structures have been optimized using DFT based two-layer ONIOM hybrid calculations. The nature of interactions has been investigated in detail using an interaction energy partitioning technique. The effects of solvation on the interaction energies have also been taken into account. An inhibition mechanism during the uptake of sarin inside the ACHE cavity has been proposed from the comparison of the energetics of the ACHE···sarin and ACHE···Ach complexes.

## 1. Introduction

In recent times, there has been an upsurge in research interest on the acetylcholinesterase (ACHE) inhibition properties of organophosphorus (OP) compounds. The nerve gases, in this respect, have drawn special interest because of their highly toxic characteristics.[1] The regulation of the concentration of the neurotransmitter acetylcholine (Ach) through strong ACHE inhibition has been related to the toxic behavior of these molecules.[1]

It is well-known that the physiological reaction catalyzed by ACHE is the hydrolysis of Ach. This reaction proceeds, after reversible substrate binding, through successive acylation and deacylation steps.[2]

$$\mathrm{ACHE} + \mathrm{S} \rightleftharpoons \mathrm{ACHE{-}S} \rightarrow \mathrm{F} + \mathrm{P} \rightarrow \mathrm{ACHE} + \mathrm{Q}$$

ACHE, S, ACHE−S, and F refer to free enzyme, free substrate, the Michaelis complex, and the enzyme intermediate, respectively. P and Q are successive choline and acetate products. This reaction takes place inside the active cavity of ACHE, and crystallographic studies characterize this cavity as a deep and narrow gorge (∼20 Å), which penetrates halfway into the enzyme.[3,4] About 40% of the inner surface of the inner gorge is lined by 14 aromatic residues.[5] It presumably facilitates the two-dimensional diffusion of Ach to the active site,[3] accommodates the substrate in the ACHE−S complex, and is involved in the allosteric modulation of catalysis.[5]

The active site of ACHE contains two main subsites. The esteric subsite,[3,4] which is composed of serine, histidine, and glutamic acid, lies about 4 Å from the bottom of the cleft. This site is responsible for the acylation and deacylation catalysis steps. The oxyanion of the tetrahedral intermediate interacts with the −NH group of the residues containing one alanine and two glycine moieties. There are two other subsites of ACHE,[3,4,6,7] one of which is highly aromatic in amino acid contents (glutamic acid, tryptophan, and phenylalanine). The other subsite, known as the acyl pocket, contains glycine, tryptophan, and phenylalanine residues and is responsible for the tight fit of the acetoxy methyl group. Finally, there is a peripheral subsite, located at the opening of the aromatic gorge. The main constituents are tryptophan, tyrosine, and aspartate, and this part helps the passage of Ach inside the cavity.[3,8]

The inhibition of ACHE by OP compounds involves phosphonylation of the active site at the serine residue and the formation of stable phosphonyl adducts.[9] Subsequently, an irreversibly inactivated enzyme is generated by spontaneous dephosphonylation of the OP−ACHE conjugate through a unimolecular process (aging).[10,11] Due to the tetrahedral geometry of the phosphonate inhibitor in the initial ACHES complex as well as in the covalent conjugate and the limited motion of the equatorial phosphorus substituents in the pentacoordinated transition state of the nucleophilic addition, the phosphonyl moiety in both of the adducts may face similar regions of active center structural manifold. As a result, the same interactions which govern the stability of the initial complex may also be important in facilitating a characteristic chemical transformation of the covalent OP−ACHE conjugate, the aging process.[12,13]

Several experimental[14−19] and molecular modeling[17,20−24] studies have been conducted on the enzyme−OP binding to understand the nature of their aging process, which has a direct consequence on the toxicity of the OP compounds and their ACHE inhibition properties. Studies on the rate processes of the aging of OP-inhibited human butyrylcholinesterase (hBCHE) and cholinesterase (hACHE)[17] have shown that among the nerve gases *O*,*O*-diisopropyl phosphorofluoridate (DFP), cyclosarin, and soman, the aging is fastest for the soman-inhibited complex. If the nerve agent is optically active, a particular enantiomer could be more active than the other. The mechanism of aging depends on the structure of the phosphonyl moiety of the OP compounds. In the case of soman-, sarin-, and DFP-inhibited ACHE, this process occurs through C−O bond cleavage.[14,15] Tabun (*O*-ethyl *N*,*N*-dimethyl-phosphoramidocyanide), on the other hand, has a −CN group attached to the P atom, and the

* Corresponding author. E-mail: jerzy@ccmsi.us.
[†] Jackson State University.
[‡] Wroclaw University of Technology.

10.1021/jp061497n CCC: $33.50 
Published on Web 06/20/2006

aging process occurs through P−N bond cleavage.[16] Experiments on the rate of the aging processes of different nerve agents and the crystallographic studies on their aged structures[14] have shown that such reaction occurs at pH 7.5−8.0 and the presence of one water molecule is needed to facilitate such a process. The crystallographic studies on the aged crystals of soman, sarin, and DFP[14] have further demonstrated that the OP oxygen atoms are within hydrogen bonding distances of four potential donors in the catalytic subsite of the enzyme. This suggests that the electrostatic forces significantly stabilize the aged enzyme.

Although the toxic behavior of the OP compounds (which occurs through the aging of the enzyme−OP complex) has been studied in detail, the primary process of ACHE inhibition is still not clear. The consideration of the $LD_{50}$ values of sarin (*O*-isopropyl methylphosphonofluoridate, 0.017 mg/kg of body weight)[1] and soman (1-methyl-2,2-dimethylpropylmethylphosphonofluoridate, 0.14 mg/kg)[25] shows that, to achieve such a high toxicity, these molecules should have strong competition with Ach while binding with the ACHE active site. The aging process, which is responsible for the toxic behavior of the nerve agents, depends on the stabilization of the enzyme−inhibitor complex. Detailed crystallographic[14−19] and molecular modeling[17,20−24] studies have been carried out, in this context, on the nerve agents.[14−19] It remains to be seen whether the inhibition of ACHE by these OP compounds starts earlier through the trapping of such molecules within the enzyme gorge.

The present paper contributes toward addressing this important feature of the OP binding using sarin as the representative system. A model active site has been generated from the crystal structure of the ACHE−DECA (decamethonium bromide, crystal code 1ACL)[21] complex. This is a nonaged crystal, and since the ammonium group in this complex shows Ach blocking through strong cation−$\pi$ interaction, the active site structure would be ideal to monitor the inhibition characteristics of sarin during complex formation and to compare the nature of binding with Ach. We have kept the basic skeleton of the active site fixed in its crystallographic geometry and studied the interaction of sarin and Ach at the density functional theory (DFT)[27] level under the ONIOM (Our-own N-layered Integrated Molecular Orbital and Molecular Mechanics) scheme.[28] Our results show that sarin actually competes with Ach during interaction with the active site, and we have also demonstrated how this complexation facilitates the formation of the ACHE−S complex through binding with the serine residue. The conformational preference of sarin enantiomers during binding with the active site, the physical nature of such interactions, and the effect of aqueous salvation on such binding have also been discussed.

The enzymatic system is a highly dynamic one, and our present model interaction analyses could be considered as a snapshot of the whole dynamic procedure. Since it has already been demonstrated through crystallographic studies on the hBCHE−OP complex that there is no appreciable shift in the position of the catalytic triad in the aged and nonaged conjugates,[15] our model interaction study using a fixed active site is quite reasonable for comparing the interaction of Ach and sarin with ACHE.

## 2. Methods of Computation

**(a) Geometry Optimization.** The active cavity of ACHE, as obtained from the crystal structure of the *Torpedo californica*−DECA complex,[26] is shown in Figure 1. The cavity is made neutral by terminating it with hydrogen atoms at the appropriate positions. The interaction energies of Ach and sarin with the active cavity were calculated by generating the optimized geometry of the respective complexes through

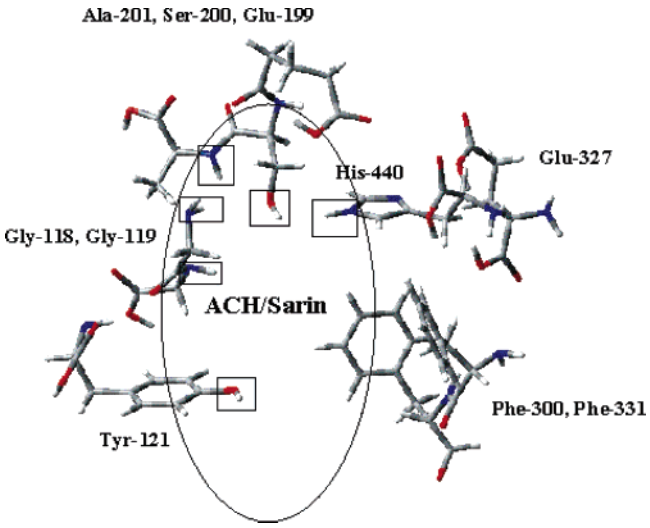


**Figure 1.** Model active cavity of ACHE from crystallographic data. The cavity is indicated by a ring, and the atoms within squares are considered as high level atoms, along with the substrate or inhibitor for the two-layer ONIOM hybrid calculations. See the method section for details.

ONIOM hybrid calculations.[28−30] Different orientations of Ach and sarin were considered for generating the complex geometry. The model ACHE−substrate complexes, thus generated, are weakly bound (not chemically bound) systems and are used for comparison of the interaction energies of the substrates with the enzyme cavity.

Two-level ONIOM hybrid calculations have been carried out for the geometry optimization of the complex using DFT,[27] which has used Becke's three-parameter functional[31] together with the local correlation part by Vosko et al.[32] and the nonlocal part by Lee, Yang, and Parr[33] (in short B3LYP). The 6-31++G-(d,p) basis sets have been used for the higher level atoms. The substrate/inhibitor is always considered at the higher level, since we are interested in their orientation within the cavity during interaction. The hydrogen atoms and the attached main atoms of the active cavity, which are marked inside squares in Figure 1, are also treated at the higher level. They could be potential hydrogen bonding sites for the substrate/inhibitor. The rest of the ACHE active cavity elements are treated at the lower level (using 3-21G(d) basis sets), as they are not involved in any direct interaction with the substrate/inhibitor. The basic skeleton of the active cavity is always kept fixed, while the substrate/inhibitor geometry with respect to this fixed skeleton has been optimized. Since the hydrogen positions were generated artificially from the crystal structure, they were also allowed to relax during geometry optimization.[34]

The effect of solvent on the calculated structures has been taken into account at the DFT/B3LYP level using a polarized continuum model with a conductor-like screening reaction field (COSMO).[35] The electrostatic properties of these complexes have been compared using the molecular electrostatic potential (MEP) surfaces generated on the isodensity surfaces of the respective complexes.

**(b) Nature of Interactions through an Energy Partitioning Technique.** The interaction energies were obtained from the optimized structure using the DFT/B3LYP and Møller−Plesset second-order perturbation (MP2) theories.[36] The active cavity of ACHE (Figure 1) could be described in terms of five distinct fragments, namely, Ala-201-Ser-200-Glu-199 (fragment $X_1$), Gly-118-Gly-119 (fragment $X_2$), His-440-Glu-327 (fragment $X_3$), Phe-330-Phe-331 (fragment $X_4$), and Tyr-121 (fragment

**SCHEME 1**

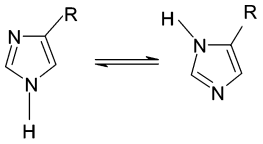

**(A)** **(B)**

$X_5$). Since these fragments are well separated in space, the total interaction energy [$\Delta E_{int}$(total)] for the ACHE (cavity)−substrate/inhibitor (S, sarin or Ach) interaction is calculated as a sum of the individual two-body interaction energy [$\Delta E_i(X_i-S)$][37] terms.

$$\Delta E_{int}(\text{total}) = \sum_{i=1-5} \Delta E_i(X_i-S) \quad (1)$$

It will be shown in the Results and Discussion section that this approximation for the total interaction energy is quite reasonable, as the three-body and higher-body interaction energy[37] contributions are not significant. All of the interaction energy calculations are carried out using 6-31++G(d,p) basis sets with counterpoise corrections.[38]

The intermolecular interactions were further analyzed using a hybrid variational−perturbational interaction energy decomposition scheme.[39] In this approach, the self-consistent field (SCF) interaction energy is partitioned into first-order electrostatic ($\epsilon_{el}^{(10)}$), Heitler−London exchange ($\epsilon_{ex}^{HL}$), and higher-order delocalization ($\Delta E_{del}^{HF}$) energy terms:

$$\Delta E^{HF} = \epsilon_{el}^{(10)} + \epsilon_{ex}^{HL} + \Delta E_{del}^{HF} \quad (2)$$

The electron correlation effects are taken into account by means of the MP2 theory. The $\epsilon_{MP}^{(2)}$ interaction energy term, which includes the dispersion and correlation contributions to the Hartree−Fock components, is calculated in the supermolecular approach as the difference of MP2 energy corrections of the supermolecule and the monomers (eq 3).

$$\epsilon_{MP}^{(2)} = E_{AB}^{(2)} - E_A^{(2)} - E_B^{(2)} \quad (3)$$

The energy terms on the right-hand side of eq 3 represent the difference between the MP2 and Hartree−Fock energies of the supermolecule (AB) and the monomers (A and B).

All of the interaction energy terms are calculated consistently in the dimer centered basis set and are therefore free from the basis set superposition error due to the full counterpoise correction.[38] The two-body interaction energies were further analyzed to get insight into factors that stabilize the ACHE···Ach and ACHE···sarin complexes.

The ONIOM and the interaction energy calculations at the DFT/B3LYP and MP2 levels were carried out using Gaussian 03 code.[40] The interaction energy decomposition scheme implemented in the GAMESS code[41] was used for energy partitioning analyses.[42] The molecular graphics and the MEP surfaces have been generated using the GaussView[43] and MOLDEN[44] software, respectively.

### 3. Results and Discussion

It is generally known that the hydrogen atom attached to the imidazole nitrogen of His-400 of the active ACHE cavity (Figure 1) could have two tautomeric positions,[45] as shown in Scheme 1. We designate the active cavity with structures A and B (Scheme 1) as ACHE(I) and ACHE(II), respectively. The

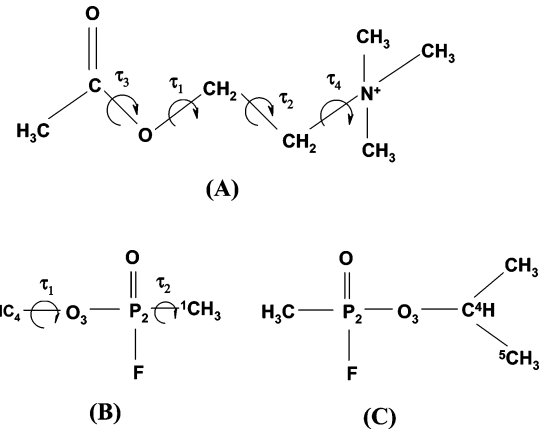

**(A)**



**(B)** **(C)**

**Figure 2.** Schematic representation of the structures of acetylcholine and sarin. Structure A is acetylcholine. The *S* and *R* enantiomers of sarin are shown as structures B and C. The torsions ($\tau_n$) in these figures are used to define the conformation of these molecules in the enzyme-bound complex (Table 4).

optimizations of the structural positions of Ach and sarin inside the ACHE active cavity have been carried out considering both the ACHE(I) and ACHE(II) structures. Since these complexes are supposed to form before Michaelis complex (ACHE−S) formation, they will be abbreviated as the ACHE···S (S, Ach or sarin) complex throughout the paper.

**(a) Interaction of Ach and Sarin with ACHE(I).** The geometry of ACHE(I)···Ach/sarin complexes has been optimized using several orientations of the substrates. The conformation of the bound substrates and their orientation inside the cavity could be described in terms of the dihedral angles ($\tau_n$, Figure 2) and the hydrogen bonding distances with the cavity atoms. Both the *R* and *S* enantiomers of sarin (Figure 2) have been considered for the interaction study. Figure 3 represents the geometry of the two best possible orientations of Ach during its interaction with the ACHE(I) cavity. Table 1 contains the results of interaction energy calculations at the DFT/B3LYP and MP2 levels. The DFT/B3LYP results show that interactions in the ACHE(I)···Ach(I) complex (Figure 3A) are much stronger than ACHE(I)···Ach(II) (Figure 3B). The interaction of Ach-(II) with ACHE(I) is rather weak.

Figure 4A and B represents the interaction of (*S*)-sarin with ACHE(I) in two different optimized orientations of the substrate. Figure 4C represents the interaction of (*R*)-sarin with ACHE-(I). The calculated values of interaction energies at the DFT/B3LYP level show that (*S*)-sarin binds strongly with ACHE(I) in the complex ACHE(I)···(*S*)-sarin(I) (Figure 4A). It is to be mentioned in this connection that we have compared the total two-body interaction energies of ACHE(I)···Ach(I) (Figure 3A) and ACHE(I)···(*S*)-sarin(I) (Figure 4A) against the respective total interaction energies at the DFT/B3LYP/3-21G(d) level. The total two-body interaction energies of ACHE(I)···Ach(I) (−14.2 kcal/mol) and ACHE(I)···(*S*)-sarin(I) (−18.6 kcal/mol) differ from the total interaction energies by 0.05 and 1.8 kcal/mol, respectively. Thus, the approximation of the total interaction energies, in these weak complexes, by the sum of total two-body interaction energies is justified.

The interaction of the ACHE(I) cavity with (*S*)-sarin in its second orientation (Figure 4B) and (*R*)-sarin (regardless of the orientation) is much weaker. Thus, sarin shows a configuration preference while interacting with the ACHE(I) active cavity. This observation is in conformity with the experiment, where the *S* enantiomer of sarin was found to be biologically active.[14] We will thus compare the nature of interactions of Ach and

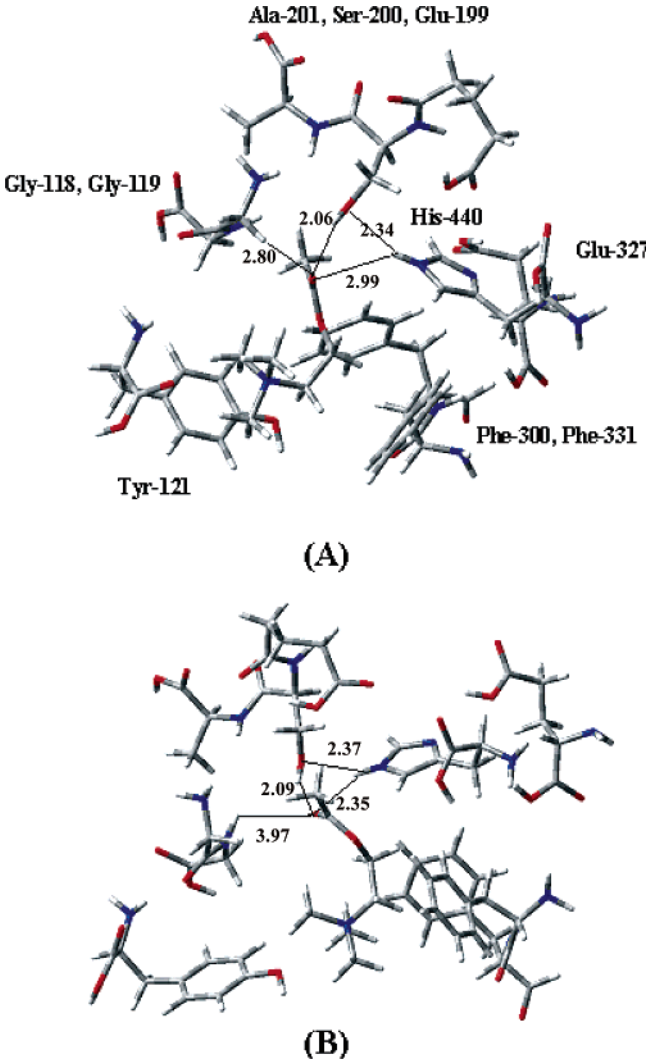


**Figure 3.** Optimized structures of (A) ACHE(I)···Ach(I) and (B) ACHE(I)···Ach(II) for the two different orientations of Ach (I and II) within the cavity. See the text for the definition of the ACHE(I) structure.

sarin with ACHE(I) in terms of the two most strongly bound systems of the respective substrate and inhibitor (Figures 3A and 4A), and we will also drop the orientation abbreviation [(I)] for them, as they will always refer to Ach(I) and (*S*)-sarin(I) for their respective complexes with ACHE(I).

The DFT/B3LYP calculations show that the interaction of (*S*)-sarin with ACHE(I) is much stronger than that with Ach. In the case of Ach, the strongest interaction is with Tyr-121. Interactions with other amino acid members are mostly repulsive except with the $X_1$ fragment, where there is a weak hydrogen bonding interaction with Ser-200. This is also evident from Figure 3A where the distance between Ser—OH···O═C (of Ach, Figure 2A) is 2.06 Å. The weak interaction ($E_{int} = -0.67$ kcal/mol) is due to the nonlinear characteristics ($\theta$(O—H···O) = 127.3°) of the hydrogen bond.

The nature of interaction of (*S*)-sarin with the ACHE(I) cavity, on the other hand, is entirely different with respect to the ACHE(I)···Ach interaction. It creates strong interaction with ACHE(I) through the hydrogen bond formation of P═O (of sarin, Figure 2) with Ser—OH (200) and the —N—H of His-440 of the $X_1$ and $X_3$ fragments, respectively. The repulsive interactions are weak (Table 1), and as a result, it appears that ACHE(I)···(*S*)-sarin interaction is much stronger than ACHE(I)···Ach interaction.

The interaction energy calculations at the DFT/B3LYP level show that the interactions of ACHE(I) with Ach/sarin are weak in nature and the optimized structures of the complexes (Figures 3A and 4A) show that there is a substantial possibility of dispersion interaction of the substrates with the cavity constituents (fragments $X_1$ to $X_5$). The interaction energy calculations at the MP2 level actually demonstrate the importance of such interactions (Table 1). Because of the dispersion and energy correlation effect ($\epsilon_{MP}^{(2)}$), the interaction of Ach with $X_1$ and $X_4$ fragments becomes stronger and its strong repulsive interaction with $X_2$ and $X_3$ (observed at the DFT/B3LYP level) fragments turns out to be much weaker. As a result, the total interaction energy is much stronger than that calculated at the DFT/B3LYP level and it is actually slightly stronger than that of the ACHE(I)···sarin complex (Table 1). We have estimated the contribution of $\epsilon_{MP}^{(2)}$ by calculating the difference of interaction energy of the complexes at the MP2 and restricted Hartree—Fock (RHF) levels using 6-31++G(d,p) basis sets. The interaction energies at the RHF level show a similar trend as DFT/B3LYP except for the fact that the ACHE(I)···Ach interaction becomes slightly repulsive (0.32 kcal/mol) due to the lack of the electron correlation effect. The estimation of $\epsilon_{MP}^{(2)}$ for the two complexes (Table 2) shows that it is higher in the case of the ACHE(I)···Ach complex and plays a major role in making the interactions of the substrate and inhibitor with ACHE(I) competitive.

**(b) Interaction of Ach and (*S*)-Sarin with ACHE(II).** The geometry of the ACHE(II)···Ach/sarin complexes has been optimized using the most preferred geometries of the ACHE(I)···Ach/(*S*)-sarin (Figures 3A and 4A) complexes. The hydrogen position of the imidazole ring (N—H) of His-440 has been shifted to its tautomeric position (Scheme 1B), and the rest of the geometric features were kept intact in the starting structures. The optimization of the substrate and inhibitor positions has been carried out using the same strategy applied for the ACHE(I)···Ach/(*S*)-sarin complexes. The optimized structures are shown in Figure 5, and the results of interaction energy calculations are presented in Table 3. Important geometric features of both Ach and (*S*)-sarin inside the ACHE(I) and ACHE(II) cavities are shown in Table 4.

The interaction energy calculations at the DFT/B3LYP level indicate that, in the case of the ACHE(II)···Ach complex (Figure 5A), the maximum contribution to the total interaction arises from the interaction of Ach with the $X_5$ fragment of the active cavity (Table 3). This part of the two-body interaction energy contribution is similar to the case of ACHE(I). Except for the $X_3$—Ach interaction (which is weakly attractive), the other contributions of the two-body interaction terms are repulsive, and thus, the total interaction energy is similar to that of the ACHE(I)—Ach complex (Table 1).

The interaction of ACHE(II) with (*S*)-sarin (DFT/B3LYP level) is totally different from the case of ACHE(I)···(*S*)-sarin (Figure 3A). Since the hydrogen bonding of P═O (of sarin, Figure 2) with the N—H of the imidazole ring (His-440) is lost here, (*S*)-sarin binds weakly with the ACHE(II) active cavity. The hydrogen bonding of P═O with Ser-OH (fragment $X_1$) is also weak (evident from Figure 5B). The contributions of the other two-body terms are either weakly repulsive ($X_3$—S, $X_5$—S; S, sarin) or attractive ($X_2$—S) (Table 5).

The results of the MP2 calculations on these complexes point to the strong contribution of the dispersion and correlation effects ($\epsilon_{MP}^{(2)}$) to the total interaction energy. Like the DFT/B3LYP results, the maximum contribution in the ACHE(II)···Ach interactions comes from the $\Delta E_5(X_5-\text{Ach})$ term. At the

**TABLE 1: Two-Body Interaction Energies [$\Delta E_{int}$(total), kcal/mol] for the ACHE(I)[a] (Active Cavity)···Substrate/Inhibitor [S, Ach and (*S*/*R*)-Sarin] Interaction at the DFT-B3LYP/6-31++G(d,p) Level [Two-Body Interaction Energy Contributions at the MP2/6-31++G(d,p) Level (in the Two Most Favorable Interactions) Are Also Included for Comparison]**

| | | $\Delta E_i(X_i-S)$ terms[c,d] (kcal/mol) | | | | | |
|---|---|---|---|---|---|---|---|
| interacting system | | $X_1-S$ | $X_2-S$ | $X_3-S$ | $X_4-S$ | $X_5-S$ | $\Delta E_{int}$(total) (kcal/mol) |
| ACHE(I)···Ach(I)[b] | DFT | −0.67 | 6.46 | 4.10 | 1.06 | −17.35 | −6.40 |
| | MP2 | −2.49 | 3.25 | 2.63 | −5.94 | −23.2 | −25.75 |
| ACHE(I)···Ach(II)[b] | DFT | −3.49 | 2.64 | 6.67 | −3.64 | −5.76 | −3.58 |
| ACHE(I)···(*S*)-sarin(I)[b] | DFT | −6.51 | 0.45 | −10.45 | −0.45 | 1.24 | −16.22 |
| | MP2 | −7.71 | −1.51 | −11.76 | −2.35 | 0.18 | −23.15 |
| ACHE···(*S*)-sarin(II)[b] | DFT | −6.64 | −0.39 | −2.94 | 3.34 | 2.14 | −4.49 |
| ACHE···(*R*)-sarin | DFT | −6.70 | 1.25 | −1.48 | 3.16 | 2.01 | −1.76 |

[a] See Scheme 1 and the text for details. [b] I and II represent the interacting systems at different orientations of the substrate/inhibitor (Ach or sarin). [c] $X_i$ ($i = 1-5$) represents the various amino acid components of the ACHE active cavity ($X_1$: Ala-201, Ser-200, Glu-199; $X_2$: Gly-118, Gly-119; $X_3$: His-440, Glu-327; $X_4$: Phe-330, Phe-331; $X_5$: Tyr-121). [d] All of the interaction energies presented here are after BSSE correction.

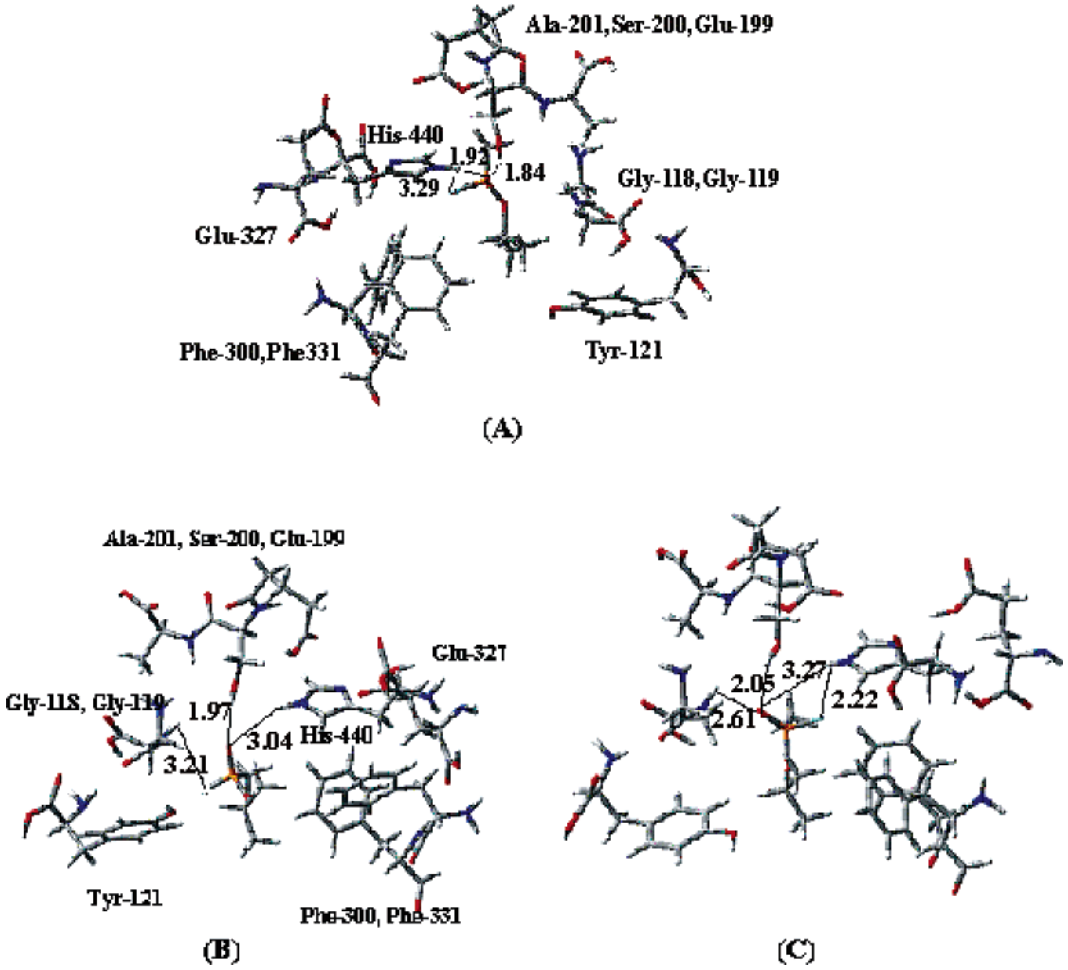


**Figure 4.** Optimized structures of (A) ACHE(I)···(*S*)-sarin(I), (B) ACHE(I)···(*S*)-sarin(II), and (C) ACHE(I)···(*R*)-sarin for the (*S*)-sarin (for two different orientations I and II) and (*R*)-sarin enantiomers, respectively.

MP2 level of theory, while the interaction energy contributions (attractive) from the $X_3-$Ach and $X_4-$Ach interactions are substantial, the repulsive contributions ($X_1-$Ach, $X_2-$Ach) are reduced due to the $\epsilon_{MP}^{(2)}$ contributions. This makes the total interaction energy of ACHE(II)···Ach similar to that of the ACHE(I)···Ach complex. Table 3 also contains the estimation of the $\epsilon_{MP}^{(2)}$ contribution obtained using the corresponding RHF calculations.

In the case of the ACHE(II)···(*S*)-sarin complex, although the contribution of $\epsilon_{MP}^{(2)}$ (Table 3) improves the total interaction energy, it is still much less than the corresponding ACHE(II)···Ach interaction. Thus, both the DFT/B3LYP and MP2 results qualitatively agree that the interaction of (*S*)-sarin with ACHE-(II) is much weaker than the ACHE(II)···Ach interaction.

**(c) Analysis of the Nature of Interactions.** Table 5 presents the interaction energy components of the ACHE(I)···S and ACHE(II)···S [S, Ach/(*S*)-sarin] complexes obtained at the RHF level. The contribution of the $\epsilon_{MP}^{(2)}$ term to these interactions has already been presented in Tables 2 and 3. These two results, together with the respective MEP isopotential surfaces, would be used to analyze the nature of interactions in these complexes.

In the case of the ACHE(I)···Ach and ACHE(II)···Ach complexes, the main contribution to the total interaction arises from the $X_5-$Ach two-body interaction. The larger contributions

**TABLE 2: Comparison of the Two-Body Interaction Energies [$\Delta E_{int}$(total), kcal/mol] for the ACHE(I) (Active Cavity)···Ach(I) and ACHE(I)···(*S*)-Sarin Interaction at the HF/6-31++G(d,p) and MP2/6-31++G(d,p) Levels for Their Most Favorable Orientations and Evaluation of the Correlation Contribution ($\epsilon_{MP}^{(2)}$, kcal/mol) to These Interaction Terms**

| | | $\Delta E_i(X_i-S)$ terms[b,c] (kcal/mol) | | | | | |
|---|---|---|---|---|---|---|---|
| interacting system[a] | | $X_1-S$ | $X_2-S$ | $X_3-S$ | $X_4-S$ | $X_5-S$ | $\Delta E_{int}$(total)[c] |
| ACHE(I)···Ach(I) | HF | −0.10 | 8.14 | 4.25 | 3.48 | −15.44 | 0.32 |
| | MP2 | −2.49 | 3.25 | 2.63 | −5.94 | −23.20 | −25.75 |
| | $\epsilon_{MP}^{(2)}$ | −2.39 | −8.40 | −1.62 | −9.42 | −7.76 | −26.07 |
| ACHE(I)···(*S*)-sarin(I) | HF | −5.61 | 0.98 | −10.47 | −1.39 | 1.84 | −14.65 |
| | MP2 | −7.71 | −1.51 | −11.76 | −2.35 | 0.18 | −23.15 |
| | $\epsilon_{MP}^{(2)}$ | −2.10 | −2.49 | −1.28 | −0.96 | 1.66 | −8.50 |

[a] I represents the interacting systems at the most favorable orientation of Ach or (*S*)-sarin. [b] See Table 1 for the definitions of $X_i$ ($i = 1-5$). [c] All of the interaction energies presented here are after BSSE correction.

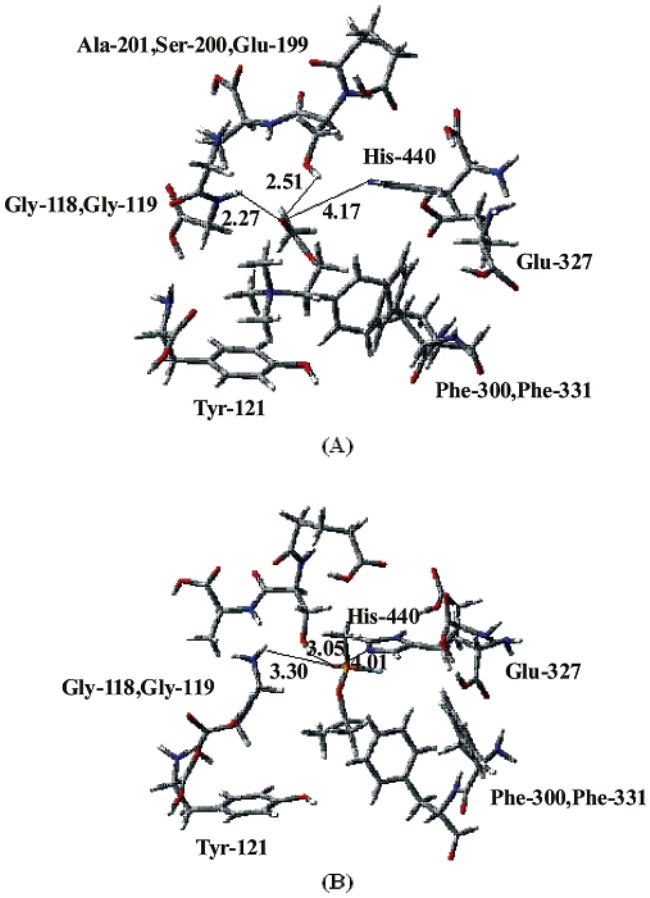


**Figure 5.** Optimized structures of (A) ACHE(II)···Ach and (B) ACHE-(II)···(*S*)-sarin. See the text for the definition of the ACHE(II) structure.

of the electrostatic ($\epsilon_{el}^{(10)}$) and delocalization ($\Delta E_{del}^{HF}$) terms make this interaction highly attractive. The contribution of the $\epsilon_{MP}^{(2)}$ component (Tables 2 and 3) increases this interaction energy further. The $X_5$ fragment corresponds to the Tyr-121 residue. The orientation of the $-N^+(CH_3)_3$ group over the aromatic ring is ideal for cation−$\pi$ interaction. However, the magnitudes of the $X_5$−Ach interaction energy of the two complexes indicate that it cannot be classified as purely cation−$\pi$, since the model cation−$\pi$ interaction energy calculated for benzene$-N^+(CH_3)_4$ is 8.1 kcal/mol at the MP2/6-31G$^{\alpha\alpha}$ level.[46] The MEP maps of the ACHE(I)···Ach and ACHE(II)···Ach complexes (Figure 6A and B) show that, apart from the simple cation−$\pi$ interaction, there is a possibility of electrostatic interactions of the $-N^+(CH_3)_3$ electron density with the side chain and the −OH group of the Tyr-121 residue of the ACHE cavity. This electrostatic effect together with the $\epsilon_{MP}^{(2)}$ term makes this interaction more attractive than the normal cation−$\pi$ interaction. In the other two-body interactions ($X_1$−Ach and $X_4$−Ach), the $\epsilon_{el}^{(10)}$ and $\Delta E_{del}^{HF}$ energies are the prominent contributions. The MP2 results in Tables 2 and 3 and the MEP maps show that the $\epsilon_{MP}^{(2)}$ contributions are also quite appreciable in these two cases. The dispersion and correlation effect actually makes the two two-body interactions attractive in nature. The electrostatic terms for the rest of the two-body terms are repulsive, and because of the geometric disposition, the $\epsilon_{MP}^{(2)}$ contributions are not appreciable. Thus, although the exchange repulsion ($\epsilon_{ex}^{HL}$) and $\Delta E_{del}^{HF}$ are low, the contributions of these two-body terms are not substantial enough to make the total interaction attractive.

The structure of the ACHE(I)···(*S*)-sarin complex (Figure 4A) indicates strong hydrogen bonding interactions with the $X_1$ and $X_3$ fragments. This is actually reflected in the values of the $\epsilon_{el}^{(10)}$ and $\Delta E_{del}^{HF}$ energy components. Although the $\epsilon_{ex}^{HL}$ terms are repulsive, the other two terms, together with the $\epsilon_{MP}^{(2)}$ terms, are strong enough to make these interaction components strongly attractive. However, the magnitudes of the interaction energies (Tables 1 and 3) indicate that these are not pure hydrogen bonding interactions. The MEP isopotential surface of the ACHE(I)···(*S*)-sarin complex shows that the attractive interactions ($\epsilon_{el}^{(10)}$ and $\epsilon_{MP}^{(2)}$) are also possible from the other parts of the $X_1$−Ach and $X_3$−Ach fragments. These effects make these two-body interactions more attractive than an ordinary hydrogen bond. The contributions of the other two-body terms to the total interaction are weak and dominated by $\epsilon_{MP}^{(2)}$. The nature of these interactions is quite predictable from the calculated results and the nature of the MEP surface (Figure 6C).

The nature of interactions is totally changed in the ACHE-(II)···(*S*)-sarin complex (Figure 4B). Since the interaction of P═O [of (*S*)-sarin] with the −N−H of the His-400 residue is lost in this case, the complex becomes a weakly bound system. The results in Table 5 show that in this complex the electrostatic terms are quite important. This is enhanced by the $\epsilon_{MP}^{(2)}$ terms (Table 3), but they are not significantly high. This is quite evident from the geometry (Figure 4A, Table 4) as well as the MEP surface (Figure 6D) of the complex. The higher stabilization, which could be achieved through these two contributions, is reduced by the repulsive effects of the $\epsilon_{ex}^{HL}$ terms. As a result, the total interaction energy in this complex is much less than that in the ACHE(II)···Ach complex.

**(d) Effect of Aqueous Solvation.** The experiments on ACHE-mediated Ach hydrolysis or the inhibition by nerve agents predict that the reaction should take place at a certain pH range (usually ∼8.0),[15] and thus, it would be interesting to investigate the change of the nature of interactions in these complexes due to solvation. Since we are keeping the structure of the ACHE cavity fixed, the direct estimation of the solvent effect on the total interaction or the dispersion effect would be inaccurate. We can, of course, qualitatively predict the change of electrostatic interaction in different dielectric media. This is

**TABLE 3: Two-Body Interaction Energies [$\Delta E_{int}$(total), kcal/mol] for the ACHE(II)[a] (Active Cavity)−Substrate/Inhibitor (S, Ach or Sarin) Interaction at the DFT/B3LYP, MP2, and HF [6-31++G(d,p)] Levels [Correlation Contributions ($\epsilon_{MP}^{(2)}$, kcal/mol) to the Two-Body Interaction Energies Are Also Presented from the MP2 and HF Results]**

| | | $\Delta E_i(X_i-S)$ terms[c,d] (kcal/mol) | | | | | |
|---|---|---|---|---|---|---|---|
| interacting system[b] | | $X_1-S$ | $X_2-S$ | $X_3-S$ | $X_4-S$ | $X_5-S$ | $\Delta E_{int}$(total)[d] |
| ACHE(II)···Ach | DFT | 2.69 | 6.81 | −1.30 | 1.14 | −17.13 | −7.79 |
| | MP2 | 0.75 | 3.48 | −3.03 | −5.70 | −23.21 | −27.71 |
| | HF | 3.52 | 8.74 | −0.98 | 3.48 | −15.56 | −0.80 |
| | $\epsilon_{MP}^{(2)}$ | −2.77 | −5.26 | −2.05 | −9.18 | −7.65 | −26.91 |
| ACHE(II)···(*S*)-sarin | DFT | −1.93 | −1.28 | 1.48 | −0.43 | 0.58 | −1.58 |
| | MP2 | −3.14 | −2.69 | 0.22 | −2.45 | −0.30 | −8.36 |
| | HF | −1.91 | −1.08 | 0.82 | −0.47 | 1.04 | 0.21 |
| | $\epsilon_{MP}^{(2)}$ | −1.23 | −1.61 | −1.60 | −1.98 | −1.34 | −8.57 |

[a] ACHE cavity with the alternate N−H position of the His-440 structure (Scheme 1). See the text for details. [b] See Table 1 for the orientation of the Ach or srarin. [c] See Table 1 for the definitions of $X_i$ ($i = 1-5$). [d] All of the interaction energies presented here are after BSSE correction.

**TABLE 4: Dihedral Angles ($\tau_n$, deg) Defining the Conformation of Ach and (*S*)-Sarin and the Important Interacting Distances (Å) between the Substrate/Inhibitor and the Amino Acid Residues in the ACHE(I)−S and ACHE(II)−S Complexes**

| geometric parameter | Ach complex[a] I | Ach complex[a] II | geometric parameter | (*S*)-sarin complex[b] I | (*S*)-sarin complex[b] II |
|---|---|---|---|---|---|
| $\tau_1$ | 117.5 | 109.8 | $\tau_1$ | −92.7 | −106.1 |
| $\tau_2$ | −74.0 | −77.3 | $\tau_2$ | −161.9 | −178.7 |
| $\tau_3$ | 174.7 | 172.8 | P═O[e]···H−O−Ser | 1.84 | 3.05 |
| $\tau_4$ | −166.4 | −166.7 | P═O[e]···H−N(His) | 1.92 | |
| >C═O[c]···H−O−Ser | 2.06 | 2.51 | P═O[e]···N(His) | | 3.30 |
| >C═O[c]···H−N(Gly[d]) | 2.99 | | P═O[e]···H−N(Gly[f]) | | 4.01 |
| >C═O[c]···H−N(His) | 2.80 | 2.77 | P−F[e]···H−N(His) | 3.29 | |
| >C═O[c]···N(His) | | 4.17 | | | |

[a] The ACHE(I)···Ach(I) and ACHE(II)···Ach(I) complexes are represented as I and II in this table. See the text for details. [b] The ACHE(I)···(*S*)-sarin and ACHE(II)···(*S*)-sarin complexes are represented as I and II in the table. See the text for details. [c] >C═O of the Ach part. See Figures 3A and 5A for details. [d] Gly-118 residue of the cavity. [e] P−O and P−F part of (*S*)-sarin. See Figures 4A and 5B for details. [f] Gly-119 residue of the cavity.

**TABLE 5: Two-Body Interaction Energy Decomposition Components (6-31++G(d,p), kcal/mol) of ACHE···Ach and ACHE···(*S*)-Sarin for Their Most Favorable Orientations**

| | | two-body components | | | | | |
|---|---|---|---|---|---|---|---|
| ACHE−S complex[a] | interaction energy component[b] | $X_1-S$ | $X_2-S$ | $X_3-S$ | $X_4-S$ | $X_5-S$ | $\sum\Delta E_i^{HF}$[c] (kcal/mol) |
| ACHE(I)···Ach(I) | $\epsilon_{el}^{(10)}$ | −7.58 | 5.58 | 4.82 | −6.08 | −33.31 | |
| | $\epsilon_{ex}^{HL}$ | 9.63 | 3.99 | 0.37 | 14.33 | 29.48 | |
| | $\Delta E_{del}^{HF}$ | −2.16 | −1.43 | −0.95 | −4.77 | −11.61 | |
| | $\Delta E_i^{HF}$ | −0.10 | 8.14 | 4.24 | 3.48 | −15.44 | 0.32 |
| ACHE(I)···(*S*)-sarin(I) | $\epsilon_{el}^{(10)}$ | −14.19 | −1.31 | −17.99 | −1.37 | −2.92 | |
| | $\epsilon_{ex}^{HL}$ | 13.66 | 2.74 | 12.45 | 0.13 | 5.65 | |
| | $\Delta E_{del}^{HF}$ | −5.08 | −0.45 | −4.94 | −0.14 | −0.91 | |
| | $\Delta E_i^{HF}$ | −5.61 | 0.98 | −10.48 | −1.39 | 1.83 | −14.66 |
| ACHE(II)···Ach | $\epsilon_{el}^{(10)}$ | −0.79 | 3.43 | −0.29 | −6.31 | −32.11 | |
| | $\epsilon_{ex}^{HL}$ | 5.50 | 7.27 | 0.22 | 14.30 | 27.53 | |
| | $\Delta E_{del}^{HF}$ | −1.19 | −1.96 | −0.91 | −4.51 | −10.98 | |
| | $\Delta E_i^{HF}$ | 3.52 | 8.74 | −0.98 | 3.49 | −15.56 | −0.80 |
| ACHE(II)···(*S*)-sarin | $\epsilon_{el}^{(10)}$ | −2.74 | −3.50 | −1.70 | −1.56 | −1.44 | |
| | $\epsilon_{ex}^{HL}$ | 1.33 | 3.43 | 4.38 | 1.37 | 2.98 | |
| | $\Delta E_{del}^{HF}$ | −0.51 | −1.02 | −0.85 | −0.28 | −0.51 | |
| | $\Delta E_i^{HF}$ | −1.91 | −1.08 | 1.82 | −0.47 | 1.04 | 0.21 |

[a] See Tables 1 and 3 for the definition of the complex systems. [b] See the text for the definition of the energy components. [c] Total two-body interaction energy at the RHF level.

quite important here, as electrostatic interaction has been found to be a major contributing factor to account for the nature of interactions in both the ACHE(I)···S and ACHE(II)···S (S, Ach/(*S*)-sarin) complexes.

The charges on different atoms have been calculated at the DFT/B3LYP (6-31++G(d,p) basis sets) level using the COSMO model,[35] and the electrostatic interaction energies have been computed from the calculated atomic charges using standard classical expression of electrostatic interaction. The calculations are performed on the two-body terms ($X_i-S$, $i = 1-5$) and then summed up to approximate the total interaction.

Figure 7 shows the change of electrostatic interactions ($\Delta E_{int}^{elec}$) in the ACHE(I)···S and ACHE(II)···S complexes in different dielectric media. The calculated $\Delta E_{int}^{elec}$ values are vertical in nature, as the geometries of the complexes were not relaxed. The $\Delta E_{int}^{elec}$ curves show that the ACHE(I)···Ach and ACHE(II)···Ach interactions become weaker due to an increase in the dielectric constant ($\epsilon$) of the medium. Since the main contributing interactions in these complexes are of the cation−$\pi$ type, the results show weakening of this interaction with increasing $\epsilon$. This observation is consistent with the previous calculations.[47−50] This weakening of interaction is probably the

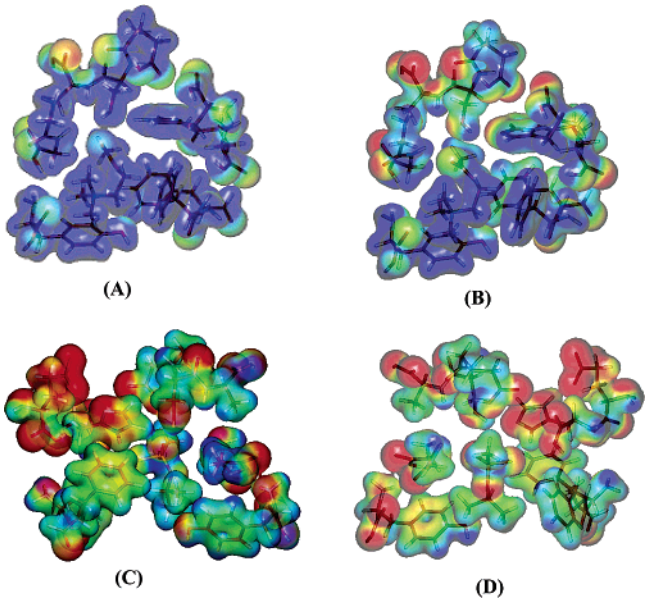


**Figure 6.** Calculated MEP on the isodensity surfaces of the (A) ACHE(I)···Ach(I), (B) ACHE(II)···Ach, (C) ACHE(I)···(*S*)-sarin(I), and (D) ACHE(I)···(*S*)-sarin complexes. The various colored regions on the surfaces are deep blue (highly positive, >0.1 au), light blue (<0.1 au and >0.05 au), green (0.0 au), yellow (< −0.1 au and > −0.05 au), and red (≥0.1 au). The minimum negative MEP values of the substrate are within the range −20 to −10 kcal/mol (greenish yellow region), while it is around −50 kcal/mol (reddish yellow region) for the inhibitor.

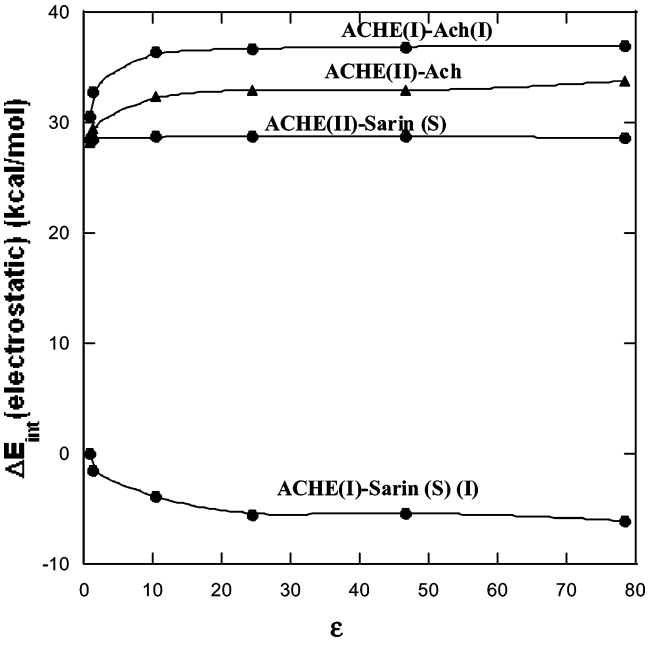


**Figure 7.** Variation of the electrostatic interaction energies [$\Delta E_{int}$-(electrostatic)] of the ACHE(I)···Ach(I), ACHE(II)···Ach, ACHE(I)···(*S*)-sarin(I), and ACHE(II)···(*S*)-sarin complexes in different dielectric ($\epsilon$) media. The electrostatic interaction energy of the ACHE(I)···(*S*)-sarin(I) complex in $\epsilon = 1$ is considered as zero, and the rest of the interaction energies are plotted relative to this zero value.

driving force to start the Michaelis complex formation, as it will allow the $CH_3(CO)O$ part of Ach to come close to the catalytic triad (Ser-200, His-440, Glu-327) of the ACHE cavity.

ACHE(I)···(*S*)-sarin interactions are increased with an increase of $\epsilon$, while in ACHE(II)···(*S*)-sarin $E_{int}^{elec}$ remains more or less constant. The main ACHE(I)···(*S*)-sarin interactions are of the hydrogen bonding type. These interactions are thus increased with an increase of $\epsilon$. Thus ACHE(I)···(*S*)-sarin interactions could even become stronger than ACHE(I)···Ach with the increasing $\epsilon$ value of the solvent medium.

**SCHEME 2**

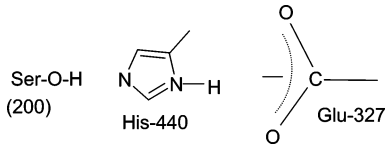


**(e) ACHE Inhibition of Sarin.** The analyses of the interactions in the considered complexes indicate that the interaction between the ACHE active cavity and the substrate/inhibitor (S, Ach/sarin) forms a weak complex prior to Michaelis complex formation. Recently, Casida and Quistad[51] have proposed such a trapping process prior to Michaelis complex formation for the ACHE inhibition by organophosphorus compounds. A comparison of the ACHE(I)···S and ACHE(II)···S structures with those of the Michaelis complex available in the literature[22,52] shows that they are formed during the pre-Michaelis complex formation. In the ACHE(I)···S complexes, the bindings of substrates are competitive, but the binding characteristic of sarin is different from Ach. Sarin actually blocks the Ser-200 and His-440 sites through hydrogen bonding, while Ach binds through cation−$\pi$ interaction with the Tyr-121 residue of the active cavity. The solvation effect is also important during such an inhibition process, as water molecules are found inside the crystal structures of many nerve agent complexes of ACHE.[14−16] The electrostatic interaction studies in different solvents have shown that this interaction increases in the ACHE(I)···(*S*)-sarin complex and is reduced in the case of the Ach complex (Figure 7). Thus, sarin physically blocks the catalytic triad part of the ACHE(I) structure through competitive binding with Ach to start the inhibition process.

The interactions in the ACHE(II)···S complexes are not competitive for Ach and (*S*)-sarin. (*S*)-Sarin binds in a much weaker way, while the nature of interactions with Ach remains more or less the same with respect to the ACHE(I)···Ach complex. During solvation, the electrostatic interactions in the ACHE(II)···Ach complex become weaker (Figure 7), while the ACHE(II)···(*S*)-sarin interactions are not changed. This weakening of interaction is important, as it might control the binding mechanism of the substrates with the Ser−OH of the catalytic triad for the formation of the Michaelis complex. In the following paragraphs, the role of the two structures (ACHE(I)···S and ACHE(II)···S) in the ACHE inhibition by sarin will be discussed in more detail.

It is generally accepted that the formation of the Michaelis complex requires the side chain −COOH group of the Glu-327 residue of the catalytic triad (Scheme 2) in the anionic form.[22,50] ACHE(II) is the ideal structure for such ionization. Energy calculations on the anionic forms (through the Glu-327 side chain −COOH dissociation) of the ACHE(I)···S and ACHE(II)···S complexes in aqueous media (COSMO model, DFT/B3LYP/3-21G(d)) show that the conversion of the ACHE(I)···S complex to ACHE(II)···S is energetically feasible and energy separation between the (*S*)-sarin complexes is lower than in the case of Ach (Table 6). The anion structures were kept the same as their corresponding neutral complexes. Since the crystallographic studies on the ACHE−nerve agent complexes have shown that the relative positions of the catalytic triad do not change during the hydrolysis reaction steps,[14,15] these single point energy calculations, although qualitative in calculating the energy separations of the anions, would generate chemically meaningful clarification of the studied phenomena.

**TABLE 6: Energy Separation ($\Delta E_s$)[a] between the ACHE(I)···S and ACHE(II)···S Complexes and Their Anions and Glu-327 Dissociation Energy of the Neutral Complexes,[a] in an Aqueous Medium, Using the DFT/B3LYP/COSMO (3-21G(d) Basis Set) Level of Calculations**

| ACHE−S complex | $\Delta E_s$ (kcal/mol) | Glu-327 ionization energy[b,c] (kcal/mol) | scaled ionization energy[d] (kcal/mol) |
|---|---|---|---|
| ACHE(I)···Ach(I) | 0.00 | 38.3 | 11.5 |
| ACHE(II)···Ach | 10.03 | 31.8 | 10.5 |
| ACHE(I)···(*S*)-sarin(I) | 0.00 | 45.3 | 14.9 |
| ACHE(II)···(*S*)-sarin | 13.63 | 32.7 | 10.7 |
| [ACHE(I)···Ach(I)]$^-$ | 0.00 | | |
| [ACHE(II)−Ach]$^-$ | 2.04 | | |
| [ACHE(I)···(*S*)-sarin(I)]$^-$ | 0.00 | | |
| [ACHE(II)···(*S*)-sarin]$^-$ | 1.02 | | |

[a] Since the energy parameters are calculated in an aqueous medium using the DFT/B3LYP/COSMO model, they could be approximated as respective free energy ($\Delta G$) values. [b] The ionization energy is calculated for the side chain COOH group of the Glu-327. [c] The ionization energy is calculated for the equilibrium as described in the text. [d] The scale factor used is 0.33. See the text for details.

We have calculated the energies of the ACHE(I)···S and ACHE(II)···S complexes to test whether they are energetically convertible in the solvent medium ($\epsilon = 78.4$). The calculations have been performed through the COSMO model using DFT/B3LYP/3-21G(d) calculations. The results contained in Table 5 show that ACHE(I)···S structures are of lower energy and not convertible to the ACHE(II)···S structures. Although the energy separations in Table 5 are not quantitative (at such a low basis set), the results are qualitatively correct. Now, if it could be shown that the formation of the ACHE(I)···S and ACHE(II)···S anions from the neutral complexes is energetically feasible, we can propose a mechanism for the inhibition property of sarin in the pre-Michaelis complex formation stage, which connects the involvement of the ACHE(I)···S and ACHE(II)···S complexes.

Table 6 contains the proton dissociation energies of the ACHE(I)···S and ACHE(II)···S complexes calculated through the COSMO model using the DFT/B3LYP/3-21G(d) level of theory. The dissociation energies were calculated using the following equilibrium scheme.

$$\text{ACHE}\cdots\text{S} + \text{H}_2\text{O} \rightleftharpoons [\text{ACHE}\cdots\text{S}]^- + \text{H}_3\text{O}^+ \qquad (4)$$

The calculated dissociation energies as listed in Table 6 are too high to predict any ionization. Tomasi and co-workers[53] have shown earlier that the predicted p$K_a$ values of the carboxylic acids are quite off from the experimental results, if the continuum model is used. Reliable p$K_a$ values could be predicted from the correlation equation obtained through the fitting of experimental and calculated results.[53] For amino acids, no such correlation is available, but we can generate a scale factor from the calculated and experimental values of the glutamic acid dissociation energy and use it to predict the dissociation energies of the ACHE−S complexes. Using the experimental p$K_a$ of glutamic acid for the side chain −COOH group (4.07), the dissociation energy turns out to be 7.9 kcal/mol[54] for the following equilibrium:

$$\text{Glu} + \text{H}_2\text{O} \rightleftharpoons \text{Glu}^- + \text{H}_3\text{O}^+ \qquad (5)$$

Considering the geometry of the Glu-327 of the active cavity, the calculated glutamic acid dissociation energy for equilibrium 5 is 24.1 kcal/mol. It leads to a scale factor of 0.33, and the scaled dissociation energies for the ACHE···S complexes are more realistic (Table 6). Thus, these calculations show that the ionization of the ACHE···S complexes is feasible and we can write the following transformations during the pre-Michaelis complex formation for the sarin and Ach complexes.

$$\text{ACHE(I)}\cdots\text{sarin} \rightarrow [\text{ACHE(I)}\cdots\text{sarin}]^- \rightarrow [\text{ACHE(II)}\cdots\text{sarin}]^-$$

$$\text{ACHE(I)}\cdots\text{Ach} \rightarrow [\text{ACHE(I)}\cdots\text{Ach}]^- \rightarrow [\text{ACHE(II)}\cdots\text{Ach}]^- \qquad (6)$$

The strong ACHE inhibition property of sarin starts during the pre-Michaelis weak complex formation (trapping), and it is a mixed effect arising from the competitive binding of this inhibitor with Ach inside the active cavity and the ease of anion formation of the ACHE···inhibitor complex to start the Michaelis complex formation. These two factors are explained below in more detail.

In the ACHE(I)···S complex, sarin competes with Ach during binding with the cavity. It is evident from the interaction energy values in Table 1. The nature of interactions shows that sarin blocks the catalytic triad through hydrogen bonding. The anion formation results show that the generation of the ACHE(II)···S anion is feasible for both of the complexes through the transformations in eq 6. Since we have kept the anion structures the same as their neutral forms, the interactions within the cavity could be considered similar in both forms. Interaction in the ACHE(II)···(*S*)-sarin complex is thus weaker than that for ACHE(II)···Ach. Although solvation weakens the ACHE(II)···Ach interaction, still it is stronger than that in the ACHE(II)···sarin complex. Sarin can thus compete with Ach to start the formation of the Michaelis complex through binding with the Ser-200 residue of the catalytic triad.

The crystallographic studies on the aged ACHE−nerve agent complexes have shown that His-440 of the catalytic triad forms a protonated structure that includes a strong hydrogen bond with the P═O bond of the aged nerve gas and results in irreversible enzyme inhibition.[14,15] Although in the ACHE(I)···(*S*)-sarin complex the inhibitor forms a hydrogen bond with His-440, it is not too strong to stop the anion formation and transformation to the corresponding tautomeric form [ACHE(II)···(*S*)-sarin anion]. The energy calculations in this respect, although qualitative in nature, support this fact. The ACHE(I)···(*S*)-sarin also lacks the proper structural requirements to irreversibly block the catalytic triad. Thus, this model study could be considered as a possible explanation of the inhibition mechanism occurring during the uptake of sarin inside the cavity. The inhibition during binding is well investigated in recent crystallographic studies.[14−16] Thus, the present study would be quite helpful to generate a more complete picture of the inhibition mechanism of sarin.

## 4. Conclusions

The nature of interactions of sarin (both the *R* and *S* enantiomers) with a model ACHE active cavity (from crystallographic data) has been studied using the ONIOM hybrid model. The interaction energies have been computed at the DFT/B3LYP and MP2 levels of theory using 6-31++G(d,p) basis sets and compared with the interaction energies of Ach with the same active cavity to explain the ACHE inhibition property of sarin. Two different cavity structures, namely, ACHE(I) and ACHE(II), have been designed considering the two tautomeric forms of the His-440 residue.

The results show that when the cavity is electrically neutral, the sarin interaction is competitive with Ach in the ACHE(I)···S [S, Ach/(*S*)-sarin] complex. The interaction of the *R* enantiomer of sarin with the active cavity was found to be very weak. The interaction of (*S*)-sarin in the ACHE(II)···S complex is weak and not competitive with Ach. Although the ACHE(II) structure has a proper orientation of the catalytic triad structure to execute the enzymatic property, the ACHE(II)−S structures are not energetically favorable. Moreover, solvation reduces the electrostatic interaction between the active cavity and substrate in the ACHE(I/II)···Ach complexes. This interaction is enhanced in the ACHE(I)···(*S*)-sarin complex, while the ACHE(II)···(*S*)-sarin interaction is unaffected with the change in the dielectric constant of the medium.

On the basis of the above analyses, it is proposed that sarin executes its inhibition property through primary blockage of the catalytic triad in the ACHE(I)···(*S*)-sarin complex. The complex is then transformed to the anionic form, which is responsible for the Michaelis complex formation (ACHE(II)···S type). Since in this complex (*S*)-sarin interacts weakly with the cavity, it can compete with Ach (where the interaction also weakens due to solvation) for the Michaelis complex formation. The proposed mechanism could be considered as inhibition during the uptake of sarin inside the cavity, and it generates a clearer picture of inhibition when the binding inhibition mechanism is taken into account from the recent experimental studies.

**Acknowledgment.** This research was supported in part by JSU and Wroclaw University of Technology, Poland, DOD support through ERDC Grant No. W912MZ-04-2-0002, and the Army High Performance Computing Research Center under the auspices of the Department of the Army, Army Research Laboratory cooperative agreement number DAAH04-95-2-0003/contract number DAAH04-95-C-0008. This work does not necessarily reflect the policy of the government, and no official endorsement should be inferred. We would like to thank the Mississippi Center for Supercomputing Research, Poznan and Wroclaw Supercomputing and Networking Centers, and the Interdisciplinary Center for Mathematical and Computational Modeling of Warsaw University for a generous allotment of computer time.

**Supporting Information Available:** A comparison of the orientation of (*S*)-sarin inside the ACHE cavity with the fixed cavity geometry (from crystallographic results) and the fully optimized cavity geometry (Figure 1s) and their calculated interaction energies (Table 1s). This material is available free of charge via the Internet at http://pubs.acs.org.

## References and Notes

(1) Toy, A. D.; Walsh, D. W. *Phophorus Chemistry in Everyday Living*, 2nd ed.; American Chemical Society: Washington, DC, 1987.

(2) Malany, S.; Sawai, M.; Sikorski, S. R.; Seravalli, J.; Quinn, D. M.; Radić, Z.; Taylor, P.; Kronman, C.; Velan, B.; Shafferman, A. *J. Am. Chem. Soc*. **2000**, *122*, 2981.

(3) Sussman, J. L.; Harel, M.; Frowlow, F.; Oefner, C.; Goodman, A.; Toker, L.; Silman, I. *Science* **1991**, *253*, 871.

(4) Harel, M.; Quinn, D. M.; Nair, H. K.; Silman, I.; Sussman, J. L. *J. Am. Chem. Soc*. **1996**, *118*, 2340.

(5) Ariel, N.; Ordentlich, A.; Barak, D.; Bino, T.; Velan, B.; Shafferman, A.; *Biochem. J*. **1998**, *335*, 95.

(6) Gentry, M. K.; Doctor, B. P. In *Cholinesterases: Structure, Function, Mechanism, Genetics, and Cell Biology*; Mossoulie, J., Bacou, F., Bernard, E., Chattonet, A., Doctor, B. P., Quinn, D. M., Eds.; American Chemical Society: Washington, DC, 1991; p 394.

(7) Taylor, P.; Lappi, S. *Biochemistry* **1975**, *14*, 1989.

(8) Deakyne, C. A.; Mout-Ner (Moutnet), M. *J. Am. Chem. Soc*. **1999**, *121*, 1546.

(9) Taylor, P. In *Goodman and Gilman's The Pharmaceutical Basis of Therapeutics*, 10th ed.; Hardman, J. G., Limbird, L. E., Eds.; McGraw-Hill: New York, 2001; p 175.

(10) Michel, H. O.; Hackley, B. E., Jr.; Berkowitz, L.; List, G.; Hackley, E. B.; Gillian, W.; Pankau, M. *Arch. Biochem. Biophys*. **1967**, *121*, 29.

(11) Benchop, H. P.; Keijer, J. H. *Biochim. Biophys. Acta* **1966**, *128*, 586.

(12) Ordenlich, A.; Kronman, C.; Barak, D.; Stein, D.; Ariel, N.; Mercus, D.; Valen, B.; Shafferman, A. *FEBS Lett*. **1993**, *334*, 215.

(13) Hosea, W. A.; Radić, Z.; Tsigelny, I.; Berman, H. A.; Quinn, D. M.; Taylor, P. *Biochemistry* **1996**, *35*, 10995.

(14) Millard, C. B.; Kryger, G.; Ordentlich, A.; Greenblatt, H. M.; Harel, M.; Raves, M. L.; Segall, Y.; Barak, D.; Shafferman, A.; Silman, I.; Sussman, J. L. *Biochemistry* **1999**, *38*, 7032.

(15) Nachon, F.; Asojo, O. A.; Brogstahl, G. E. O.; Masson, P.; Lockridge, O. *Biochemistry* **2005**, *44*, 1154.

(16) Ekström, F.; Akfur, C.; Tunemalm, A.-K.; Lundberg, S. *Biochemistry* **2006**, *45*, 74.

(17) Ordentlich, A.; Barak, D.; Kronmann, C.; Benschop, H. P.; De Jong, L. P. A.; Ariel, N.; Barak, R.; Segall, Y.; Velan, B.; Shafferman, A. *Biochemistry* **1999**, *38*, 3055.

(18) Jennings, L. L.; Malecki, M.; Komives, E. A.; Taylor, P. *Biochemistry* **2003**, *42*, 11083.

(19) Hill, C. G.; Li, W.-S.; Thoden, J. B.; Holden, H. M.; Raushel, F. M. *J. Am. Chem. Soc*. **2003**, *125*, 8990.

(20) Ordentlich, A.; Barak, D.; Kronmann, C.; Ariel, N.; Segall, Y.; Velan, B.; Shafferman, A. *J. Biol. Chem*. **1998**, *273*, 19509.

(21) Masson, P.; Fortier, P.-L.; Albarte, C.; Froment, M.-T.; Bartels, C. F.; Lockridge, O. *Biochem. J*. **1997**, *327*, 601.

(22) Ordentlich, A.; Barak, D.; Kronmann, C.; Ariel, N.; Segall, Y.; Velan, B.; Shafferman, A. *J. Biol. Chem*. **1996**, *271*, 11953.

(23) Segall, Y.; Waysbort, D.; Barak, D.; Ariel, N.; Doctor, B. P.; Grunwald, J.; Ashani, Y. *Biochemistry* **1993**, *32*, 13441.

(24) Bencsura, A.; Enyedy, I.; Kovach, I. M. *Biochemistry* **1995**, *34*, 8989.

(25) Rump, S.; Kowalczyk, M. *J. Med. Chem. Def*. **2004**, *1*, 1.

(26) Harel, M.; Shalk, I.; Ehret-Sabatier, I.; Bouet, F.; Goeldner, M.; Hirth, C.; Axelsen, P. H.; Silman, I.; Sussman, J. L. *Proc. Natl. Acad. Sci. U.S.A.* **1993**, *90*, 9031.

(27) Parr, R. G.; Wang, W. *Density Functional Theory of Atoms and Molecules*; Oxford: New York, 1984.

(28) Vreven, T.; Morokuma, K. *Theor. Chem. Acc*. **2003**, *109*, 125.

(29) Maseras, F.; Morokuma, K. *J. Comput. Chem*. **1995**, *16*, 1170.

(30) Vreven, T.; Morokuma, K. *J. Comput. Chem*. **2000**, *16*, 1419.

(31) Becke, A. D. *J. Chem. Phys*. **1993**, *98*, 5648.

(32) Vosko, S. H.; Wilk, L.; Nusair, M. *Can. J. Phys*. **1980**, *58*, 1200.

(33) Lee, C.; Wang, W.; Parr, R. G. *Phys. Rev. B* **1988**, *37*, 785.

(34) Full optimization of the active cavity is another alternative to locate the orientation of the substrate/inhibitor inside the cavity. However, such an optimization might lead to an unphysical situation in the present case. A case study has been made in the case of ACHE···(*S*)-sarin interaction with the fully optimized active cavity (chosen from the present study). The results are compared with those of the fixed cavity geometry (Figure 1s and Table 1s in the Supporting Information) to vindicate the validity of our present approach.

(35) Barone, V.; Cossi, M. *J. Phys. Chem. A* **1998**, *102*, 1995.

(36) Møller, C.; Plesset, M. *Phys. Rev*. **1943**, *46*, 618.

(37) Kaplan, I. G. *Theory of Molecular Interactions*; Elsevier: Amsterdam, The Netherlands, 1986.

(38) Boys, S. F.; Bernardi, F. *Mol. Phys*. **1970**, *19*, 553.

(39) Sokalski, W. A.; Roszak, S.; Pecul, K. *Chem. Phys. Lett*. **1988**, *153*, 153.

(40) Frisch, M. J.; Trucks, G. W.; Schlegel, H. B.; Scuseria, G. E.; Robb, M. A.; Cheeseman, J. R.; Montgomery, J. A., Jr.; Vreven, T.; Kudin, K. N.; Burant, J. C.; Millam, J. M.; Iyengar, S. S.; Tomasi, J.; Barone, V.; Mennucci, B.; Cossi, M.; Scalmani, G.; Rega, N.; Petersson, G. A.; Nakatsuji, H.; Hada, M.; Ehara, M.; Toyota, K.; Fukuda, R.; Hasegawa, J.; Ishida, M.; Nakajima, T.; Honda, Y.; Kitao, O.; Nakai, H.; Klene, M.; Li, X.; Knox, J. E.; Hratchian, H. P.; Cross, J. B.; Bakken, V.; Adamo, C.; Jaramillo, J.; Gomperts, R.; Stratmann, R. E.; Yazyev, O.; Austin, A. J.; Cammi, R.; Pomelli, C.; Ochterski, J. W.; Ayala, P. Y.; Morokuma, K.; Voth, G. A.; Salvador, P.; Dannenberg, J. J.; Zakrzewski, V. G.; Dapprich, S.; Daniels, A. D.; Strain, M. C.; Farkas, O.; Malick, D. K.; Rabuck, A. D.; Raghavachari, K.; Foresman, J. B.; Ortiz, J. V.; Cui, Q.; Baboul, A. G.; Clifford, S.; Cioslowski, J.; Stefanov, B. B.; Liu, G.; Liashenko, A.; Piskorz, P.; Komaromi, I.; Martin, R. L.; Fox, D. J.; Keith, T.; Al-Laham, M. A.; Peng, C. Y.; Nanayakkara, A.; Challacombe, M.; Gill, P. M. W.; Johnson, B.; Chen, W.; Wong, M. W.; Gonzalez, C.; Pople, J. A. *Gaussian 03*, revision C.02; Gaussian, Inc.: Wallingford, CT, 2004.

(41) Schmidt, M. W.; Baldridge, K. K.; Boatz, J. A.; et al. *J. Comput. Chem*. **1993**, *14*, 1347.

(42) Gora, R. W. *EDS V2.1.2 package*; Wroclaw, Poland, and Jackson, MS, 1988−2003.

(43) *GaussView, Commercial Molecular graphics software*; Gaussian, Inc.: Wallingford, CT, 2004.
(44) Schaftenaar, G.; Noordik, J. H. *J. Comput.-Aided Mol. Des.* **2000**, *14*, 123.
(45) Sudmier, J. L.; Bradshaw, E. M.; Haddad, K. E. C.; Day, R. M.; Thalhauser, C. J.; Bullock, P. A.; Bachovchin, W. W. *J. Am. Chem. Soc*. **2003**, *125*, 8430.
(46) Pullman, A.; Berthier, G.; Savinelli, R. *J. Am. Chem. Soc*. **1998**, *120*, 8553.
(47) Duffy, E. M.; Kowalczyk, P. J.; Jorgensen, W. L. *J. Am. Chem. Soc*. **1993**, *115*, 9271.
(48) Ma, J. C.; Dougherty, D. A. *Chem. Rev*. **1997**, *97*, 1303.
(49) Gallivan, J. P.; Dougherty, A. A. *Proc. Natl. Acad. Sci. U.S.A.* **1999**, *96*, 9459.
(50) Minoux, H.; Chipot, C. *J. Am. Chem. Soc.* **1999**, *121*, 10366.
(51) Casida, J. E.; Quistad, G. B. *Chem. Res. Toxicol.* **2004**, *17*, 983.
(52) Wlodek, S. T.; Antosiewicz, J.; Briggs, M. J. *J. Am. Chem. Soc*. **1997**, *119*, 8154.
(53) Achüürmann, G.; Cossi, M.; Barone, V.; Tomasi, J. *J. Phys. Chem. A* **1998**, *102*, 6706.
(54) The ionization energy is calculated using the relation $\Delta G = 5.71 \mathrm{p}K_a + 9.96$ kJ/mol (as described in ref 50).